Research Article | Vol. 7, No. 9 | 1 Sep 2017 | OPTICAL MATERIALS EXPRESS 3408
Optical Materials EXPRESS

Phase transformation under direct laser writing in a YAG single crystal

A. G. OKHRIMCHUK,[1,2,*] A. S. LIPATIEV,[1] E. V. ZHARIKOV,[3,4] G. ORLOVA,[5] V. MEZENTSEV,[6] AND P. G. KAZANSKY[1,7]

[1]*International Centre of Laser Technologies, D. Mendeleev University of Chemical Technology of Russia, Geroev Panfilovtsev st., 20, Moscow 125480, Russia*
[2]*Fiber Optics Research Centre of Russian Academy of Sciences, Vavilov Str. 38, Moscow 119991, Russia*
[3]*D.Mendeleev University of Chemical Technology of Russia, Miusskaya Sq. 9, Moscow 125047, Russia*
[4]*Prokhorov General Physics Institute of Russian Academy of Sciences, Vavilov Str. 38, Moscow 119991, Russia*
[5]*R&D Stelmakh's Polyus Institute, Vvedensky Str. 3, Moscow 117342, Russia*
[6]*Aston Institute of Photonic Technologies, Aston University, Birmingham B4 7ET, UK*
[7]*Optoelectronics Research Centre, University of Southampton, Southampton SO17 1BJ, UK*
**a.okhrim@yandex.ru*

Abstract: The transformation from $Y_3Al_5O_{12}$ to perovskite $YAlO_3$ crystal phase was observed during ultrafast laser writing in the bulk of a $Y_3Al_5O_{12}$ single crystal. The control of the phase transformation was demonstrated by tuning parameters of laser writing. The phenomenon is interpreted in terms of structural changes in the overheated garnet melt under laser heating followed by rapid solidification, and at least 1-ms dwell time of overheated melt is required to start spontaneous crystallization. The appearance of the perovskite phase was confirmed by Raman spectroscopy, quantitative phase and polarization microscopies.

OCIS codes: (160.3380) Laser materials; (190.7110) Ultrafast nonlinear optics; (230.4000) Microstructure fabrication.

References and links

1. V. Koubassov, F. J. Laprise, F. Thereberge, E. Forster, R. Sauerbrey, B. Muller, U. Glatzel, and S. L. Chin, "Ultrafast laser-induced melting of glass," Appl. Phys., A Mater. Sci. Process. **79**(3), 499–505 (2004).
2. B. Yu, B. Chen, X. Yang, J. Qiu, X. Jiang, C. Zhu, and K. Hirao, "Study of crystal formation in borate, niobate, and titanate glasses irradiated by femtosecond laser pulses," J. Opt. Soc. Am. B **21**(1), 83 (2004).
3. B. Lu, B. Yu, B. Chen, X. Yan, J. Qiu, X. Jiang, and C. Zhu, "Study of crystal formation in titanate glass irradiated by 800 nm femtosecond laser pulse," J. Cryst. Growth **285**(1-2), 76–80 (2005).
4. X. Du, H. Zhang, C. Cheng, S. Zhou, F. Zhang, Y. Yu, G. Dong, and J. Qiu, "Space-selective precipitation of ZnO crystals in glass by using high repetition rate femtosecond laser irradiation," Opt. Express **22**(15), 17908–17914 (2014).
5. M. Zhong, Y. Du, H. Ma, Y. Han, B. Lu, Y. Dai, and X. Zeng, "Crystalline phase distribution of $Dy_2(MoO_4)_3$ in glass induced by 250 kHz femtosecond laser irradiation," Opt. Mater. Express **2**(8), 1156 (2012).
6. J. Cao, B. Poumellec, L. Mazerolles, F. Brisset, A.-L. Helbert, S. Surble, X. He, and M. Lancry, "Nanoscale Phase Separation in Lithium Niobium Silicate Glass by Femtosecond Laser Irradiation," J. Am. Ceram. Soc. **8**, 1–8 (2016).
7. A. Vailionis, E. G. Gamaly, V. Mizeikis, W. Yang, A. V. Rode, and S. Juodkazis, "Evidence of superdense aluminium synthesized by ultrafast microexplosion," Nat. Commun. **2**, 445 (2011).
8. A. G. Okhrimchuk, V. K. Mezentsev, H. Schmitz, M. Dubov, and I. Bennion, "Cascaded nonlinear absorption of femtosecond laser pulses in dielectrics," Laser Phys. **19**(7), 1415–1422 (2009).
9. A. Okhrimchuk, "Femtosecond Fabrication of Waveguides in Ion-Doped Laser Crystals," in *Coherence and Ultrashort Pulse Laser Emission*, F. J. Duarte, ed. (InTech, 2010).
10. J. P. Hurrell, S. P. S. Porto, I. F. Chang, S. S. Mitra, and R. P. Bauman, "Optical Phonons of Yttrium Aluminum Garnet," Phys. Rev. **173**(3), 851–856 (1968).
11. A. Chopelas, "Single-crystal Raman spectra of $YAlO_3$ and $GdAlO_3$: comparison to several orthorhombic ABO_3 perovskites," Phys. Chem. Miner. **38**(9), 709–726 (2011).
12. S. P. S. Porto and R. S. Krishnan, "Raman Effect of Corundum," J. of Chem. Phys. **47**, 1009(1967).
13. A. Mortensen, D. H. Christensen, O. F. Nielsen, and E. Pedersen, "Raman Spectra of Amorphous Al_2O_3 and Al_2O_3/MoO_3 Obtained by Visible and Infrared Excitation," J. Raman Specroscopy **22**(1), 47–49 (1991).

#295960 https://doi.org/10.1364/OME.7.003408
Journal © 2017 Received 16 May 2017; revised 18 Jul 2017; accepted 19 Jul 2017; published 29 Aug 2017

Optical Materials EXPRESS

14. C. J. Bellair, C. L. Curl, B. E. Allman, P. J. Harris, A. Roberts, L. M. D. Delbridge, and K. A. Nugent, "Quantitative Phase Amplitude Microscopy IV: Imaging Thick Specimens," J. Microsc. **214**(1), 62–69 (2004).
15. M. Gervais, S. Le Floch, J. C. Riffiet, J. Coutures, and J. P. Coutures, "Effect of the Melt Temperature on the Solidification Process of Liquid Garnets $Ln_3Al_5O_{12}$ (Ln = Dy, Y, and Lu)," J. Amer. Am. Ceram. Soc. **75**(11), 3166–3168 (1992).
16. J. L. Caslavsky and D. J. Viechnicki, "Melting behaviour and metastability of yttrium aluminium garnet (YAG) and $YAlO_3$ determined by optical differential thermal analysis," J. Mater. Sci. **15**(7), 1709–1718 (1980).
17. B. Cockayne and B. Lent, "Complexity in The Solidification Behaviour of Molten Y3Al5012," J. Cryst. Growth **46**(3), 371–378 (1979).
18. N. Padture and P. Klemens, "Low thermal conductivity in garnets," J. Am. Ceram. Soc. **80**(4), 1018–1020 (1997).
19. P. G. Kazansky, W. Yang, E. Bricchi, J. Bovatsek, A. Arai, Y. Shimotsuma, K. Miura, and K. Hirao, ""Quill" writing with ultrashort light pulses in transparent optical materials," Appl. Phys. Lett. **90**(15), 151120 (2007).
20. K. W. Martin and L. G. Deshazer, "Indices of Refraction of the Biaxial Crystal $YAlO_3$," Appl. Opt. **12**(5), 941–943 (1973).
21. R. W. Dixon, "Photoelastic Properties of Selected Materials and Their Relevance for Applications to Acoustic Light Modulators and Scanners," J. Appl. Phys. **38**(13), 5149–5153 (1967).
22. M. Bass, ed., *Handbook of Optics, Vol. 2.* (McGraw_Hill, 1995).
23. P. Nayar, X. Y. Zhu, F. Yang, M. Lu, G. Lakshminarayana, X. P. Liu, Y. F. Chen, and I. V. Kityk, "Fabrication and characterization of highly luminescent Er^{3+}:Al_2O_3 thin films with optimized growth parameters," Opt. Mater. (Amst) **60**, 57–61 (2016).

1. Introduction

Femtosecond laser inscription has rapidly progressed into an enabling technology for micro- and nano- scale phase transformation between the amorphous and the crystalline phases in glass matrixes for applications ranging from nonlinear frequency conversion to lasing in micro volumes [1–6]. Photonics structures inscribed in crystalline matrices are advantageous compared to those in glasses due to higher thermal conductivity of crystals, that facilitates thermal management during propagation of high intensity pulses, and thus, have advantages in applications of laser optics. In particular, it was reported that tight focusing of the femtosecond laser beam inside sapphire single crystal led to formation of metallic aluminum phase in nano-scale volume [7]. However, earlier the phase transitions between dielectric crystalline phases or any phase transformations on a microscopic scale have never been observed. In this paper we report on the phase transformation in $Y_3Al_5O_{12}$ (YAG) single crystals into $YAlO_3$ (YAP) crystals at microscopic scale. This phenomenon enables developing a range of photonic structures such as crystalline waveguides with high refractive index contrast for high peak and average power applications. Since YAG and YAP crystals have high segregation coefficients for rare-earth ions, the discovered effect of transformation paves the way for developing high power waveguide lasers with cavity length less than 1 cm.

2. Laser writing of tracks

Femtosecond laser beam generated by Pharos-SP oscillator-amplifier system (Light Conversion) at 1028 nm wavelength and pulse duration of 180 fs at 1 MHz repetition rate was focused in the volume of YAG single crystal sample 180 μm beneath its polished surface. In order to diminish Kerr self-focusing and to obtain smooth tracks of modification we used the lens system with strong astigmatic focusing consisted of the cylindrical divergence lens (f = −1000 mm) and the near infrared microscope objective (Olympus, LCPLN50XIR, NA = 0.65) [8] (Fig. 1). It produced two beam waists of elliptical cross-sections as viewed along the laser beam. For the laser pulse energy exceeding the modification threshold a considerable part of it gets absorbed in the vicinity of the beam waist next to the objective. Further optical microscopic investigations of track's end view images revealed, that the remote waist does not facilitate any modification in the sample due the lack of the energy to exceed the modification threshold after initial absorption at the first beam waist. The elliptical waist had a small diameter of 1.3 μm (at e^{-2} level of peak intensity) and a large diameter of 17 μm calculated for a diffraction of a Gaussian beam and a confocal length was around 7 μm. A crystal sample, the target for fs laser inscription, was mounted on the air-bearing translation

Optical Materials EXPRESS

stage (Aerotech, ABL 1000) and moved perpendicular to the laser beam axis along the large diameter of the elliptical beam waist.

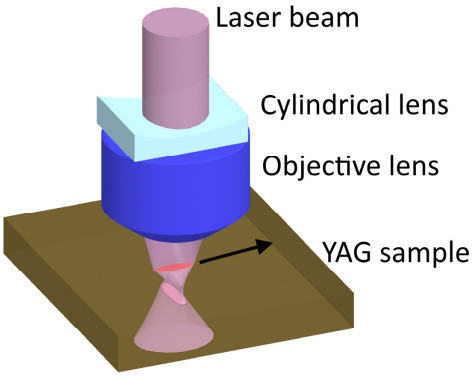

Fig. 1. Optical scheme of focusing setup for laser writing and transmittance measurement.

Two differently doped YAG crystals were investigated in the experiments, namely YAG:Cr^{4+} doped with Cr(0.4at.%) and Mg(0.25at.%), and YAG:Yb^{3+}(15at.%). The YAG:Cr^{4+} crystal had absorption as high as 0.7 cm^{-1} at 1030 nm due to 4-fold coordinated Cr^{4+} ions. An attenuator based on a half-wave plate and Brewster film polarizer (Watt Pilot, Altechna) was used to control the power of laser beam entering the crystal sample. Birefringence induced by laser writing was investigated with polarization microscope that provided with 2D mapping of retardance and azimuth of slow axis (Abrio Microbirefringence).

3. Birefringence in tracks

First of all series of tracks were inscribed in YAG:Cr^{4+} crystal under the average power incident on the sample P_{in} of 0.51 W (Fig. 2). The tracks were differed by the writing velocity and polarization of laser beam and were inscribed in such a way that moving of the beam waist began and finished at a position out of the sample. Each track has 3 sections, two of them were written along "Y" with the indicated velocity, and one was written along "X" under velocity of 0.1 mm/s.

The tracks written with the velocity of 0.2–1.6 mm/s have inhomogeneous irregular intrinsic structure, which is easily observable due to light scattering with the upright microscope in the bright field regime. Width of these tracks is about 5–10 μm, that is, it is considerably larger than the beam waist small diameter. Micro cracks are occasionally observed in the vicinity of these tracks. In opposite, tracks written with the velocity higher 1.6 mm/s have both narrow smooth homogeneous sections similar to those that composed depressed cladding waveguide structures [9], and wide sections with irregular structure similar to those written with low velocities. The smooth sections have low contrast in the bright field regime, and they are almost indistinguishable (Fig. 2).

Optical Materials EXPRESS

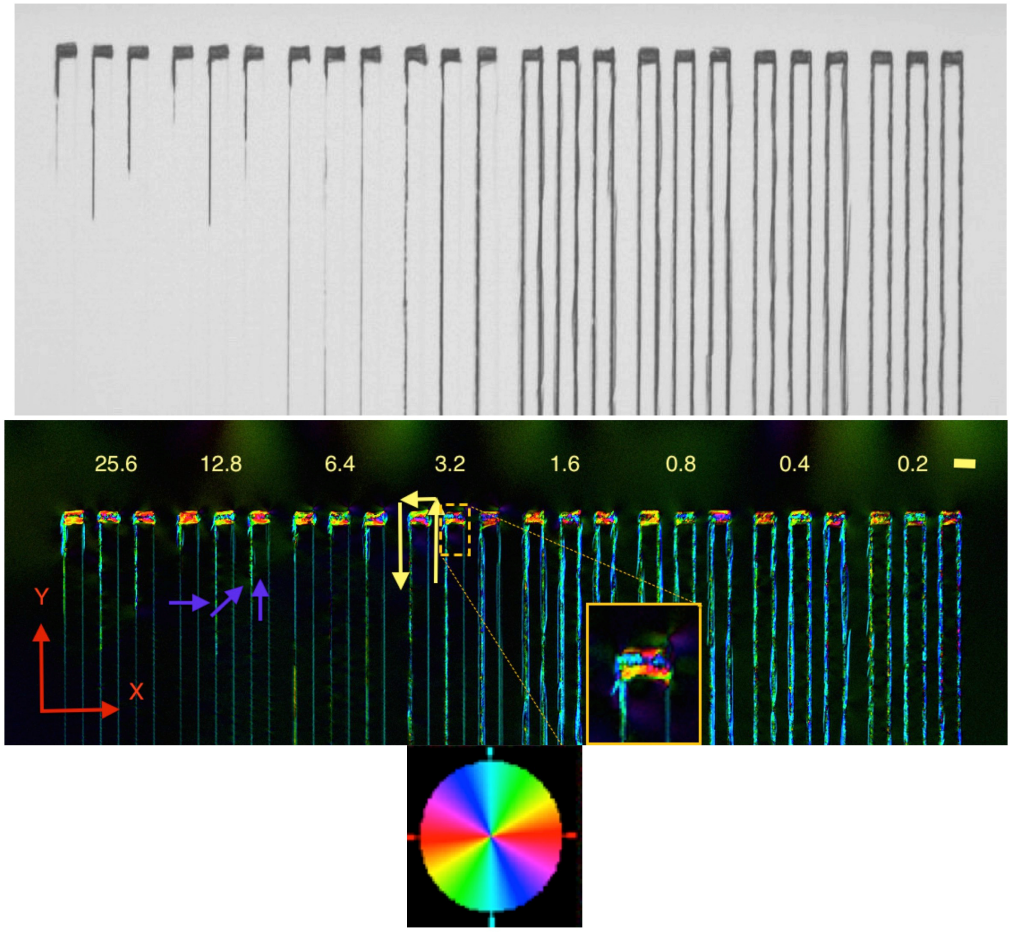

Fig. 2. Bright field microscope picture (on the top) and birefringence mapping (below) of track written in YAG:Cr^{4+} crystal under laser beam power P_{in} of 0.51 W. Color codes direction of the slow axis as indicated in the legend at the bottom, brightness codes retardance in relative units. Moving of the beam waist began and finished out of the sample during writing of each track. The yellow arrows indicate directions of writing that are repeated for each track. The digits indicate the writing velocity V [mm/s] for the sections of tracks directed along Y-axis, and it is the same for each group of the tree adjacent tracks. The writing velocity is 0.1 mm/s for all the sections along the X-axis. The blue arrows indicate directions of polarization that are constant within a track. Directions of polarizations are periodically repeated from left to right over 3 tracks. The scale bar length is 20 μm.

It was found that the birefringence mapping of tracks is correlated with pictures obtained in bright field regime. Tracks written with velocity below 2 mm/s are qualitatively different compared to the tracks written with higher velocity. It is notable that in every track two sections written along "Y" axis under velocity higher than 2 mm/s have strongly different birefringence and homogeneity. Namely, first sections are smooth and have uniform retardance of birefringence along its length with the slow axis oriented along a track. The third sections of tracks, that is the sections written along "Y" axis after the sections written along "X" axis, and all other tracks written with the velocity below 1.6 mm/s exhibit contrasted behavior, showing a non-uniform retardance and randomly fluctuating azimuth of the slow axis along and perpendicular to a track. Thus retardance had strongly non-monotonic dependence on the writing velocity.

Optical Materials EXPRESS

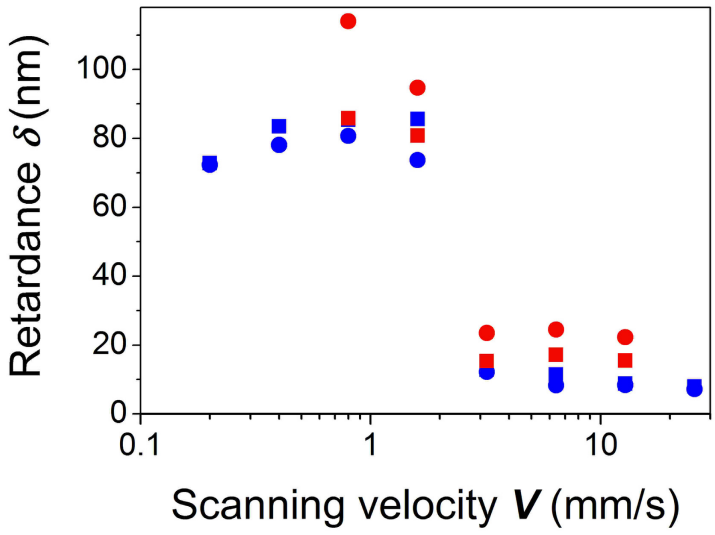

Fig. 3. Dependency of the magnitude of retardance in a track on the scanning velocity for YAG:Cr^{4+} crystal under laser beam power $\boldsymbol{P_{in}}$ of 0.51 W (blue points), and in YAG:Yb^{3+} crystal under laser beam power of 0.52 W (red points). The direction of polarization was either parallel (squares) or perpendicular (circles) to a track. The measurement wavelength is equaled to 543 nm.

Dependence of retardance magnitude in the first "Y"-sections of tracks written in YAG:Cr^{4+} crystal (Fig. 2) is shown in Fig. 3. Similar measurements were made for YAG:Yb^{3+} crystal. The dependencies have pronounced kinks at the velocity near 2–3 mm/s for both YAG:Cr^{4+} and YAG:Yb^{3+} crystals.

4. Transmittance during the inscription of tracks

The power of the passed beam was measured behind the YAG:Cr^{4+} crystal while scanning velocity of the sample was varied. Power of incident laser beam P_{in} was being set in the range of 0.33-0.53 W. Such combination of writing parameters permitted to identify conditions and reasons leading for appearance of strong birefringence. The focusing optics and depth were the same as in previous section. The diameter of the sensitive area of the power meter head was 10 mm, which was about twice as large compared to the focusing objective diameter. The former was placed apart 5 mm behind the sample, that is, practically at the same distance, as the objective working distance (4 mm). Hence the entire beam hits the power meter. Measurements were organized in such a way that the full scan path was exceeding the crystal size. The scanning velocity was decreased from 6 mm/s to zero starting at the beam entrance to the sample and finishing at the middle of the sample. Then acceleration was immediately started, and scanning velocity reached 6 mm/s at the beam exit from the sample. Thus the movement was always in the same direction during the measurements. The absorbed power P_0 was calculated by subtracting of the transmitted power from the incident power P_{in}. The results are presented in Fig. 4.

Optical Materials EXPRESS

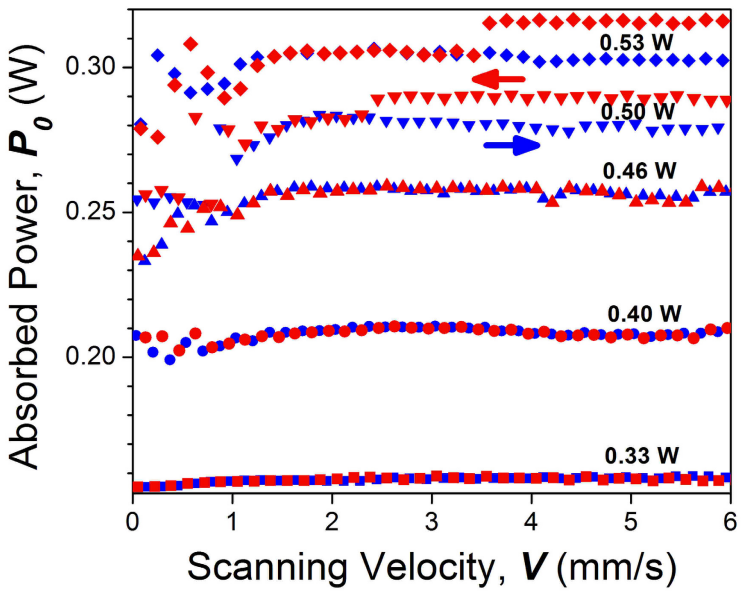

Fig. 4. Dependences of power absorbed in YAG:Cr^{4+} crystal on the scanning velocity under five different values of the incident powers P_{in} that are indicated near the dependencies curves. Red points correspond to decelerating moving, and blue points correspond to moving with positive acceleration.

5. Raman spectroscopy

Vibration spectra of track sections oriented along "Y" were investigated with Raman confocal spectrometer. The facet of an investigated crystal, that is perpendicular to these sections, was ground and polished so that tracks emerged at the crystal surface. Ar-laser beam with the wavelength of 488 nm was focused by objective lens with a numerical aperture NA = 0.7 under crystal surface at the depth of 5 μm that is similar to the Rayleigh length of the laser beam waist. Spatial resolution was defined by the beam waist diameter, which was about 0.5 μm. Backscattered light was collected by the same objective lens and detected by the cooled Andor CCD sensor. Polarized spectra of the 15×15 μm rectangular undersurface region with a track included were recorded point-by-point with a step of 0.5 μm in both transverse coordinates.

Spectra taken from unmodified regions or from the tracks written with writing speed above 3 mm/s are very analogous to spectra obtained for YAG [10], while those for scanning velocity below 2 mm/s show both the lines specific to the YAG crystal and also intense additional lines that cannot be associated with vibrations in YAG as presented in Fig. 5. It was found that the additional lines correspond to vibration of $YAlO_3$ crystal (YAP) with perovskite structure [11]. In order to make an unambiguous identification of the additional lines, we have prepared the x-cut and the y-cut plates of YAP single crystal and recorded its Raman spectra. Here we imply the crystal symmetry space group with *Pbnm* notation. Polarizing spectra of these crystals are also presented in Fig. 5 for comparison.

Optical Materials EXPRESS

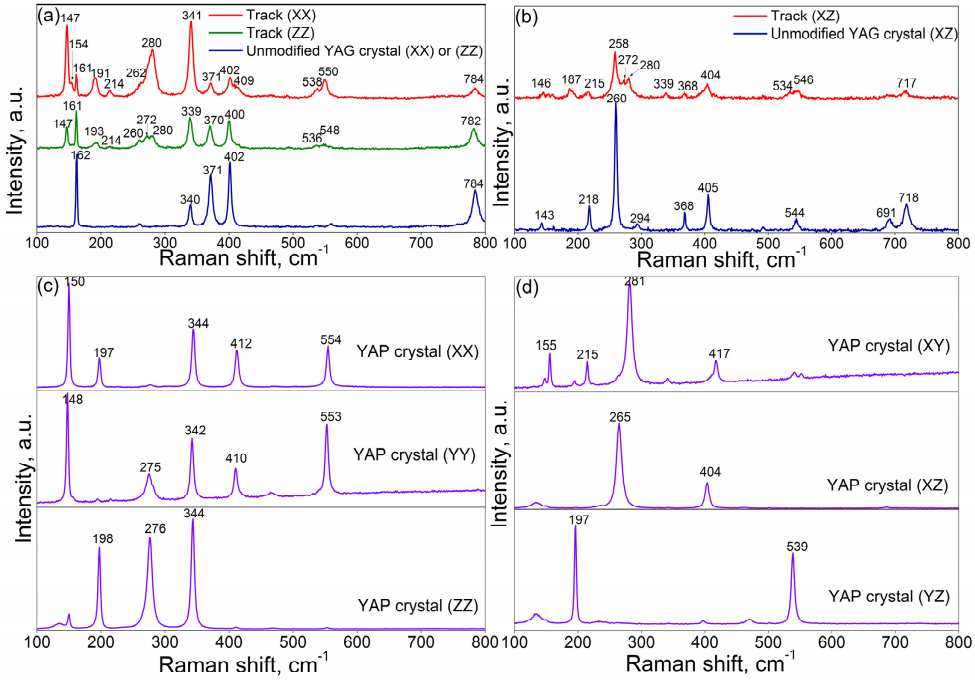

Fig. 5. Polarized Raman spectra taken under excitation in the center of the track cross-section and in the region of unmodified YAG crystal (a,b), and of YAP single crystal samples (c,d). Polarizations of excitation and registration are shown in brackets. Spectra a) and c) are for parallel polarizations, and b) and d) are for crossed polarizations. The track was inscribed at the scanning velocity of 1.6 mm/s.

It was found that most intense additional lines in the tracks written with velocity lower than 2 mm/s (147 cm^{-1}, 341 cm^{-1}) correspond to specific line in YAP single crystal with an error not exceeding 1 cm^{-1}. Positions of the weaker additional lines have a mismatch with YAP lines reaching 8 cm^{-1}, which could be due to stress arising from density change accompanying the phase transformation. This clearly shows that significant volume of YAG in the tracks is transformed to YAP according to an estimate based on relative intensities of lines corresponding to YAG and YAP phases. Inasmuch YAP contains fewer content of Al_2O_3 than YAG, a surplus of an aluminum oxide should appear in the vicinity of the YAP phase. Nevertheless we did not find any manifestation of Raman lines of the Al_2O_3 crystal phase [12]. This fact can be only explained by assuming that the surplus of Al_2O_3 gets transformed to an amorphous phase with a very broad Raman spectrum, and its intensity is insufficient for detection in our experimental setup [13].

6. Quantitative phase microscopy (QPM)

Quantitative phase microscopy (QPM) was applied to investigate 3D distribution of refractive index change in the tracks [14]. Microscopic images were captured with 14-bit CCD under illumination by unpolarized light at the wavelength of 650 nm with an objective, which had $NA = 0.9$. Depth of field D_z of the objective was less than 1 μm, and thickness of a track along direction of writing beam h was around 20 μm. Thus the microscope had enough spatial resolution to distinguish the difference in refractive index mapping in the cross-sections separated by more than 1 μm. QPM method was originally developed for 2D mapping of refractive index in a plane object under the assumption of constant refractive index along the axis of observation. However qualitative estimation of its variation along this axis could be done in our case of a non-plane object, since depth of field D_z of our lens was considerably

Optical Materials EXPRESS

less than the track thickness *h*. Thus, although we have not a possibility of measuring the absolute value of refractive index change, we assume that it is proportional to the optical path difference, defined with QPM. Profiles of refractive index change in arbitrary units under focusing at different depth are presented in Fig. 6. In order to produce QPM treatment two defocused images were captured under 1-μm shift from the focus position.

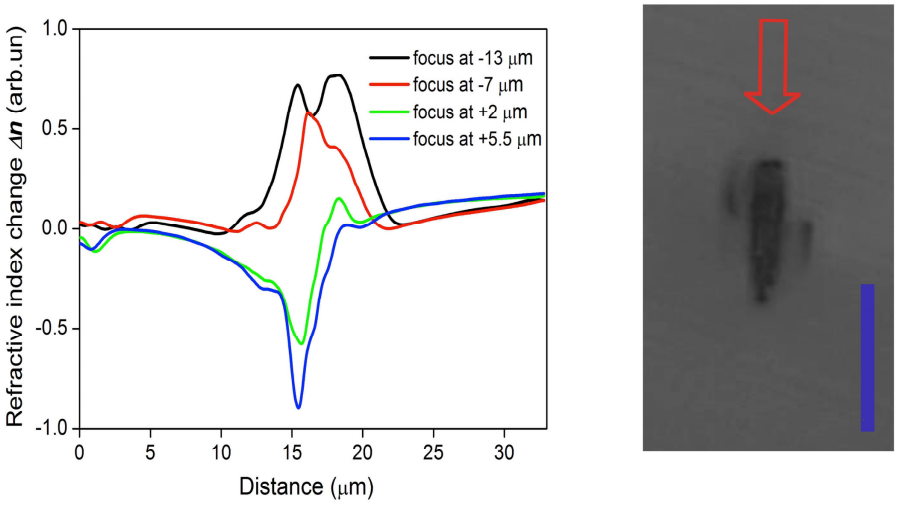

Fig. 6. Left: profiles of refractive index change in the third "Y" section of the track inscribed at the translation velocity of 3.2 mm/s. Profiles were captured perpendicular to the track and under focusing at different depth relative the crystal surface. Focus positions are indicated relative a point in the middle of the modification. Right: the end view of the track. The red arrow indicates the direction of writing beam and the viewing direction for QPM. Scale bar is 20 μm.

7. Discussions

The inscribed tracks exhibit remarkable birefringence. However, YAG crystal, the host material, has the cubic structure, which implies optical isotropy and exhibits no birefringence. There are two possible explanations of the birefringence onset in the tracks (Fig. 2,3). One is presence of stresses due to the melting and subsequent crystallization of YAG. The other is formation of compounds of non-cubic crystals in the track. YAG has been shown to crystallize either as the single garnet phase $Y_3Al_5O_{12}$ or a mixture of perovskite $YAlO_3$ and aluminum oxide α-Al_2O_3, depending on the temperature reached by the melt [15]. The perovskite phase formation during solidification of molten YAG was repeatedly observed experimentally by different authors [15–17]. In our experiments the Raman spectra unambiguously confirm formation of the perovskite phase in the tracks written with velocity lower than 2 mm/s.

When the melt temperature exceeds YAG melting point (1940°C), structural changes starting from approximately 2000°C take place in the liquid [15]. Consequently, the melt being cooled down from temperatures above 2000°C follows the crystallization path of the metastable phase diagram resulting in occurrence of YAP instead of YAG [16] according to the reaction:

$$Y_3Al_5O_{12} = 3YAlO_3 + \alpha Al_2O_3 \quad (1)$$

Optical Materials EXPRESS

We consider that femtosecond laser writing providing rapid cooling of the overheated melt fulfills the required conditions for the metastable crystallization. For the phase transformations to occur, a high enough average absorbed power of the laser beam is required to melt YAG locally. Heating the melt by about 100 degree over the melting temperature arouses disintegration the clusters of YAG structure motives existing in the melt and leads to further crystallization by metastable path presented above by reaction (1) [16]. So the lowering of the scanning velocity facilitates a longer presence of the melt at the specific point of the crystal sample and finally leads to formation of YAP phase. Figure 2 and 3 reflect final consequences of the phase transformation, while the transformation process is monitored in Fig. 4. Because of the large beam waist diameter exceeds maximum melt diameter (which is less than 5 μm as it is followed from Fig. 7 below) in our experiments, it is the averaged power absorbed partly in the melt and partly in the neighboring solid phase is depicted in Fig. 4. Thus the absorbance depends on the type of crystal phase formed at the crystallization zone, and the kinks at the velocities of 2.3 mm/s and 3.5 mm/s under corresponding incident powers P_{in} of 0.50 W and 0.53 W reflect transformation to perovskite phase. Spread of experimental points under scan velocities below 1 mm/s could be explained by scattering on increased inhomogeneity of polycrystalline structures, which are formed whether due to recrystallization of YAG phase, or transformation of YAG phase to a mixture of YAP and YAG phases.

7.1. Heat transfer analysis

In order to establish the spatial dimension, the temperature and the lifetime of the molten phase we have exploited a simplified heat model. A laser induced heat source was considered in the form of the laser radiation absorbed in the vicinity of the beam waist. The adapted heat transfer equation model was used and described in Appendix in details. The material parameters required for a heat transfer analysis are as following: specific heat capacity c_p = 0.6 J/(gK), YAG crystal density ρ = 4.5 g/cm^3, and $\kappa(T)$ = 0.03 – 0.013 W/(cm·K) is the temperature dependent thermal conductivity. The heat source is characterized by the total absorbed power $P_0(t)$.

The absorbed energy is delivered by periodic pulses with the repetition rate of 1 MHz, which makes the laser pulse train period of 1 μs. We assume that due to pronounced nonlinear nature of the femtosecond pulses absorption, the relevant heat source has form of an ellipsoid, which diameters are defined by the waist diameters and confocal length of the beam, and hence the spatial size of the heated material is around $d_s = \sqrt[3]{1.3 \cdot 17 \cdot 7} = 5\mu m$. This assumption leads to the estimate of the characteristic heat spreading time $\tau = c_p \rho d_s^2 / \kappa = 17\mu s$, where the thermal conductivity κ = 0.04 W/(cm·K) is taken at 1000 K. Hence thermal diffusion between the consecutive pulses is negligible and the heating source can be considered stationary in the laboratory system so that $P_0(t)$ = const. The averaged absorbed power was one of the experimentally measured parameters.

The thermal conductivity strongly depends on temperature in the range between the room temperature and the melting temperature. The experimental data for temperature dependence of the thermal conductivity for polycrystalline YAG suggest a very accurate fit [18]:

$$\kappa(T) = \kappa_1 + (\kappa_0 - \kappa_1)\exp\left(-\frac{T - T_\infty}{T_k}\right) \quad (2)$$

where T_∞ is a room temperature, T_k = 420 K is a fitting parameter and parameters κ_0 = 0.13 W/(cm·K) and κ_1 = 0.035 W/(cm·K) have a meaning of thermal conductivity of the crystalline YAG at room and a very high temperature respectively.

Optical Materials EXPRESS

A heat transfer problem was solved in a spherical geometry in order to establish key parameters and their principal dependencies. It turns out that a spherical symmetry allows deriving the final solution for a stationary temperature distribution in a closed analytical form. Obviously, a more realistic case of an ellipsoidal heat source would distort spherical symmetry but the major parameters scaling should stay qualitatively similar. The quantitative results in terms of spatial scales of the temperature distribution should hold in the direction with a smallest diameter of the heat source.

The main facts which are independent on a detailed spatial distribution of a heat source are i) heating regime is practically stationary and not noticeably distorted by the sample movement, ii) a critical absorbed power P_{cr} is required for the peak temperature $T_{\max}$ to reach the critical temperature T_{cr} at the center of the heat source, iii) diameter of the domain with a molten phase heated over T_{cr} strongly depends on the absorbed power in the vicinity of its critical threshold P_{cr} when it shoots to its characteristic value followed by a smooth linear growth.

The results of this analysis are presented in the following two Figures. Figure 7 shows a smooth growth of the peak temperature versus total absorbed power for different sizes of the heat source determined by the source size parameter a. Figure 8 shows the dependency of the overheated melt diameter d versus total absorbed power P_0 for different values of the heat source size. It shows a sharp rise of the overheated melt diameter d with a small excess of the absorbed power P_0 over the critical value P_{cr} when the peak temperature exceeds the critical melt temperature T_{cr}.

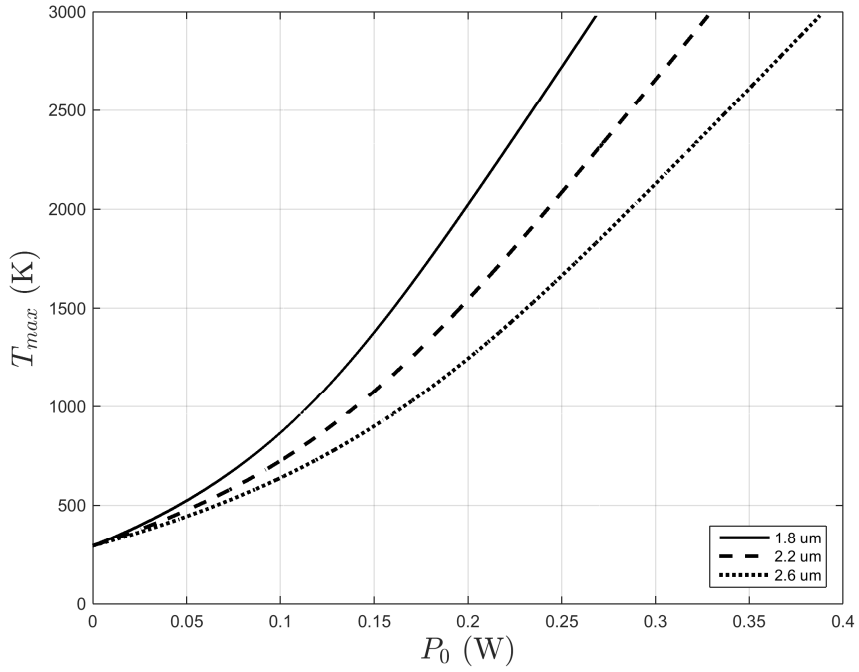

Fig. 7. Calculated dependence of the maximum temperature T_{max} reached at the center of the beam waist on the absorbed power P_0 under different size of the heat source determined by parameter a: 1.8 μm (solid line), 2.2 μm (dashed line), and 2.6 μm (dotted line).

Optical Materials EXPRESS

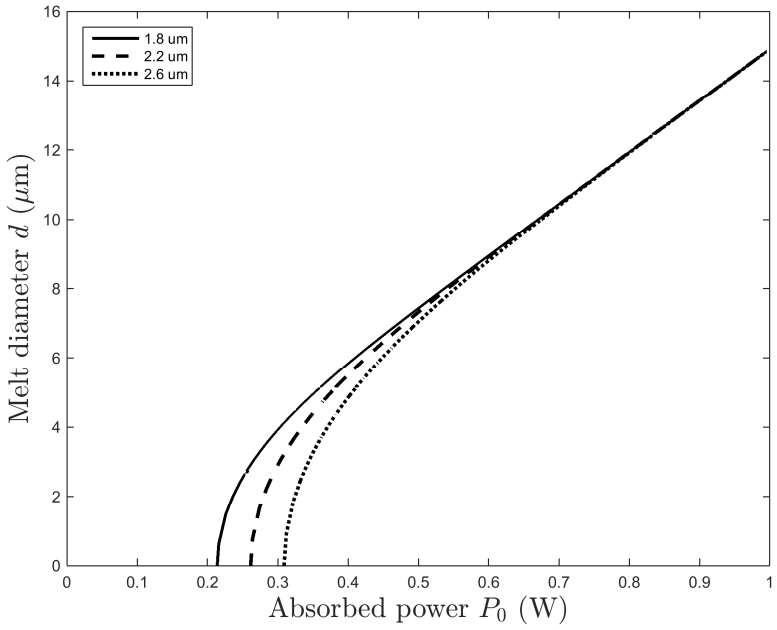

Fig. 8. The diameter of the overheated melt d versus absorbed power P_0 for different size of the heat source determined by parameter a: 1.8 μm (solid line), 2.2 μm (dashed line), and 2.6 μm (dotted line).

7.2. Analysis

The melt temperature is entirely defined by the average absorbed power, and it does not depend on the scanning velocity due to a very low Péclet number, as it was explained above. Figure 4 shows that the minimal absorbed power, required for the phase transformation is about 0.27 W. This value is in good agreement with the calculated critical power P_{cr} for the melt overheated over the melting temperature by 100 degrees for the heat source size a of 2.2 μm (Fig. 8). In Fig. 4 this corresponds to average incident beam powers P_{in} = 0.50–0.53 W. The laser beam certainly melts YAG crystal when the incident power exceeding 0.46 W, while the peak melt temperature T_{max} exceeds the melting temperature by 100 K at the critical incident power P_{in}, which is apparently should be in the range of 0.46-0.50 W. Thus the overheated melt assists laser writing of all tracks in Fig. 2,3, and the maximum melt temperature exceeds the temperature T_{cr} that is necessary for decomposition of YAG clusters at stationary melt temperature. However the last condition is still insufficient for crystallization of perovskite phase. The next key parameter controlling the phase transformation under the lack of seeding for perovskite phase is the dwell time $\boldsymbol{\tau}$ of a specific point in a track for being in the overheated melt. The scanning velocity V defines this time by formula $\tau = d/V$, where d is the diameter of overheated melting zone. Figure 8 shows a quick raise of the diameter d up to nearly 3 μm with a small excess of the absorbed power P_0 over the critical value of 0.27 W (at a = 2.2 μm). The critical scanning velocity for phase transformation without seeding is about 2-3 mm/s as followed from the results of writing with deceleration (Fig. 4) or constant velocities (Fig. 3). The relation $\tau = d/V$ immediately leads to an estimate of the maximum duration of existence of the molten phase in crystal to be about 1 ms for an absorbed power slightly exceeding the critical value of 0.27 W. Thus we estimated low limit of the melt dwell time that is necessary for complete decomposition of YAG structural motives in the melt that ensures metastable crystallization of perovskite phase without seeding.

Optical Materials EXPRESS

It is remarkable that in Fig. 4 there are no kinks in dependencies while writing with acceleration (obviously the corresponding kinks should occur at higher velocities that were not achieved in our experimental conditions). We suggest that once perovskite phase has appeared at low velocity due to metastable crystallization, it further serves as a seed and prolongs crystallization path to YAP phase even when the dwell time τ becomes below 1 ms.

Writing in different directions along "Y" at velocity exceeding 2 mm/s gives strongly different birefringence (Fig. 2). Strong birefringence was obtained with low velocity writing in a section of track parallel to "X" axis, while there is low birefringence in a section written along "Y" axis as a first section of a track. This situation is similar to writing with and without seeding correspondingly and is described in the previous paragraph. Alternatively, another interpretation of anisotropic writing may be proposed. That is, the picture is analogous to quill writing in glasses, which happens due to pulse front tilt in a writing beam [19]. However, we are inclined to the first explanation.

The transverse size of a track in the direction of inscribing beam h is nearly 20 μm. Estimation of birefringence for tracks written below 2 mm/s (as in Fig. 3), yields high value of $\Delta n = \delta / h \approx 0.005$. Such value of birefringence agrees with the birefringence of YAP crystal (n_a = 1.921, n_b = 1.9375, n_c = 1.9465 at 650 nm [20]). Random distribution of optical axis could be explained by polycrystalline nature of the YAP phase (Fig. 2). These facts lead us to conclude that the strong birefringence appeared after writing with speed below 2 mm/s is due to the presence of the YAP crystal phase.

There is small birefringence in the "Y" sections of tracks written at the speed above 3 mm/s, in which the phase transformations are not expected. We explain this birefringence by elasto-optical effect due compressive stress developed in tracks. Strain along a track is negligible due to geometrical factor, and thus the elasto-optical effect does not cause refractive index change for light polarized along a track. Refractive index change Δn due to the elasto-optical effect for perpendicular polarization can be estimated from the formula:

$$\Delta n = -\frac{1}{2} n^3 p_{11} \frac{p}{E} \tag{3}$$

where n is the refractive index of YAG, p_{11} is the diagonal component of elasto-optical tensor (p_{11} = –0.029 [21], E is Young's modulus (E = 280 GPa [22]), p is the pressure inside a track, wherein negative pressure corresponds to the compressive stress. The measured retardance gives estimation of the relative index decrease for polarization perpendicular to track of 0.001 (Fig. 2). Then calculations with Eq. (3) give $p \approx$-3 GPa. Stress of such magnitude can be clamped in the crystal, because it is still in the range of elastic deformation for YAG. Indeed the estimated pressure magnitude is as low as 1% of Young's modulus E.

Spatial separation of the YAP crystalline and the Al_2O_3 amorphous phases becomes apparent in the mapping of refractive index, which was done with QPM. Profiles of refractive index change in a first "Y" section of tracks written with velocity above 2 mm/s (Fig. 2) are similar to the previously observed profiles while writing with a low repetition rate femtosecond laser [9], where phase transformations were not observed. Refractive index change is negative for all cross sections independently on the focusing depth and has as high maximum as 0.003. In tracks written with velocities lower than 2 mm/s the sign of refractive index change depends on the focusing depth and its maximum magnitudes are rather larger. Profiles of refractive index change in cross-sections perpendicular to tracks are shown in Fig. 6. It was found that refractive index change is negative at the upper part of the track (closer to the surface) with estimation of low limit of magnitude as high as 0.01 and positive at the deeper part with the same estimation of the magnitude.

We consider that the positive index change reflects transformation to YAP phase, because this change is about to index difference between YAG (1.82) and YAP (1.92) crystals. We assume that the negative index change corresponds to decrease of the index due to occupying

Optical Materials EXPRESS

corresponding volume by amorphous phase of Al_2O_3, which could be in the range 1.65-1.70, as it was found during investigations of amorphous Al_2O_3 films [23]. Thus phase microscopy investigation reveals that YAP phase appears in the deeper part of the track that is farther from the YAG crystal surface, whereas in the upper part of the track refractive index is lower, and it could belonging to the amorphous phase of Al_2O_3, although we failed to find an aluminum oxide phase by Raman spectroscopic investigations.

8. Summary

Controlled transformation of YAG single crystal to polycrystalline perovskite $YAlO_3$ and amorphous Al_2O_3 phases were obtained under direct femtosecond laser writing with 1 MHz repetition rate in the form of a millimeter long track with a few microns size cross-section. It was found that 1 ms is the minimum time that is required to start crystallization of YAP phase without a seeding. Once the seeding is formed, the dwell time can be considerably reduced. This corresponds to increase of the scanning velocity up to 3 times while writing tracks with perovskite phase. Appearance of the perovskite phase was confirmed by Raman spectroscopy, quantitative polarization microscopy, and quantitative phase microscopy, while indication of necessary concomitant transformation to aluminum oxide phase was found with quantitative phase microscopy only. We found that the key parameter for this phenomenon to occur is the average power of the femtosecond laser beam. It should exceed the critical threshold required for producing a moving overheated melting zone in the YAG crystal. Such conditions of crystal melting ensure rapid quenching after the melting zone being passed. The observed new type of structural modification initiated by femtosecond laser writing could be demonstrated in other crystals of garnet family at least, and it opens the way of new possibilities for fabrication of photonic structures in crystals.

Appendix

The evolution of the material temperature is described by a heat equation written in the sample's coordinate system:

$$c_p\rho\frac{\partial T}{\partial t}=\nabla\kappa(T)\nabla T+p(\vec{r}-\vec{V}t,t) \tag{4}$$

where $T(\mathbf{r}, t)$ is a material temperature, V is the sample translation speed, and $p(\mathbf{r}–\mathbf{V}t)$ is a specific absorbed power defined so that the total absorbed power in the whole volume of the sample $P_0(t)$ is:

$$P_0=\int_V p(\vec{r},t)d\vec{r} \tag{5}$$

The next temporal issue in the inscription process is a movement of the heat source. In the laboratory system with $\boldsymbol{r}–\boldsymbol{V}t\rightarrow\boldsymbol{r}$ the heat source is stationary and so the temperature profile should be described with a stationary advection-diffusion equation:

$$c_p\rho\vec{V}\cdot\nabla T+\nabla\kappa(T)\cdot\nabla T+p(\vec{r})=0 \tag{6}$$

The relative role of the first two terms in this equation is determined by the dimensionless Péclet number (*Pe*), which is defined as a ratio of advective transport rate given by the first term to the thermal diffusive transport rate given by the second term. The numerical value of *Pe* number

Optical Materials EXPRESS

$$Pe = \frac{c_p \rho V d_s}{\kappa} \approx 0.01 \tag{7}$$

is rather low for the scanning velocities corresponding to the phase transformation. It shows a negligible role of the advective transport rate compared to heat diffusion rate and hence the advective term can be totally neglected as it is for zero scanning velocity. In order to get tangible results we have considered a spherically symmetric Gaussian distribution of the specific absorbed power:

$$p(\vec{r}) = \frac{P_0}{\pi^{3/2} a^3} \exp\left(-\frac{r^2}{a^2}\right) \tag{8}$$

where radius $a \cong d_s/2$.

Solution of the Eq. (4) with the boundary conditions $dT/dr\big|_{r=0} = 0$ and $T\big|_{r=\infty} = T_\infty$ yields the following transcendental equation relating temperature T and a radius r:

$$F(T) = \left(F(T_{\max}) - \frac{P_0}{2\pi^{3/2} a}\right) + \frac{P_0}{4\pi a} \frac{1}{x} erf(x) \tag{9}$$

where $erf(x)$ is the error function, $x = r/a$, and a function of temperature $F(T)$ is an integral of thermal conductivity $\kappa(T) = dF(T)/dT$. The temperature at the center $T_{\max} = T(r = 0)$ that is the maximum temperature can be found from:

$$F(T_{\max}) = F(T_\infty) + \frac{P_0}{2\pi^{3/2} a} \tag{10}$$

Results of calculations according to Eq. (9) and (10) are presented in Fig. 7. Obviously, a minimum critical power P_{cr}:

$$P_{cr} = 2\pi^{3/2} a \left(F(T_{cr}) - F(T_\infty)\right)$$

is required for the maximum temperature to reach temperature $T_{cr} = 2040°C$ that corresponds to 100-degree overheating over the melting temperature. For any absorbed power exceeding this critical value a spherical domain of a radius r_m of the overheated molten phase is formed around the center according to the transcendental equation:

$$F(T_{cr}) - F(T_\infty) - \frac{P_0}{4\sqrt{\pi} r_m} erf\left(\frac{r_m}{a}\right) = 0 \tag{11}$$

In this equation, the only fitting parameter is the source size parameter a. The results of this analysis are presented in Fig. 8.

Funding

The Ministry of Education and Science of Russian Federation (14.Z50.31.0009).

Acknowledgments

A.G. Okhrimchuk is grateful to A.A. Sobol for discussions concerning Raman spectroscopy.